Bi-allelic Mutations in *TTC21A* Induce Asthenoteratospermia in Humans and Mice

Wangjie Liu,[1,2,3,14] Xiaojin He,[4,5,6,14] Shenmin Yang,[7,8,14] Raoudha Zouari,[9] Jiaxiong Wang,[7,8] Huan Wu,[4,5,6] Zine-Eddine Kherraf,[10,11] Chunyu Liu,[1,2,3] Charles Coutton,[10,12] Rui Zhao,[1] Dongdong Tang,[4,5,6] Shuyan Tang,[1,2] Mingrong Lv,[4,5,6] Youyan Fang,[4,5,6] Weiyu Li,[1,2,3] Hong Li,[7,8] Jianyuan Zhao,[1] Xue Wang,[13] Shimin Zhao,[1,2] Jingjing Zhang,[4,5,6] Christophe Arnoult,[10] Li Jin,[1] Zhiguo Zhang,[4,5,6] Pierre F. Ray,[10,11,15] Yunxia Cao,[4,5,6,15,*] and Feng Zhang[1,2,3,4,15,*]

Male infertility is a major concern affecting human reproductive health. Asthenoteratospermia can cause male infertility through reduced motility and abnormal morphology of spermatozoa. Several genes, including *DNAH1* and some *CFAP* family members, are involved in multiple morphological abnormalities of the sperm flagella (MMAF). However, these known genes only account for approximately 60% of human MMAF cases. Here, we conducted further genetic analyses by using whole-exome sequencing in a cohort of 65 Han Chinese men with MMAF. Intriguingly, bi-allelic mutations of *TTC21A* (tetratricopeptide repeat domain 21A) were identified in three (5%) unrelated, MMAF-affected men, including two with homozygous stop-gain mutations and one with compound heterozygous mutations of *TTC21A*. Notably, these men consistently presented with MMAF and additional abnormalities of sperm head-tail conjunction. Furthermore, a homozygous *TTC21A* splicing mutation was identified in two Tunisian cases from an independent MMAF cohort. *TTC21A* is preferentially expressed in the testis and encodes an intraflagellar transport (IFT)-associated protein that possesses several tetratricopeptide repeat domains that perform functions crucial for ciliary function. To further investigate the potential roles of *TTC21A* in spermatogenesis, we generated *Ttc21a* mutant mice by using CRISPR-Cas9 technology and revealed sperm structural defects of the flagella and the connecting piece. Our consistent observations across human populations and in the mouse model strongly support the notion that bi-allelic mutations in *TTC21A* can induce asthenoteratospermia with defects of the sperm flagella and head-tail conjunction.

Human infertility is a worldwide health concern and affects in excess of 186 million people.[1] Male infertility is often caused by asthenoteratospermia, characterized by obviously decreased sperm motility and multiple morphological abnormalities of the flagella (MMAF).[2] Intraflagellar transport (IFT) is known to be essential for the development and maintenance of flagella; thus, it plays a very important role in spermatogenesis and male fertility.[3,4] IFT was first characterized in the green algae *Chlamydomonas reinhardtii* and was shown to rely on a motor-driven trafficking system that transports flagellar precursors to the site of assembly.[3,5,6] To date, many studies on model organisms have shown that IFT defects cause a range of cilia-dependent disorders and male infertility. For example, a deletion mutation affecting *Chlamydomonas IFT52* prevents flagellar formation.[7] Furthermore, germ-cell-specific *Ift140*-knockout mice are completely infertile because of sperm flagellar malformation and dramatic reductions in sperm count.[8] Notably, all of the *Ift20-*, *Ift25-,* and *Ift27*-knockout mutants in mice result in male infertility.[9–11] Despite numerous examples highlighting the relationship between IFT and flagellar formation in *Chlamydomonas* and animal models, the influence of IFT in human male infertility has not been reported.

Previous genetic studies on human MMAF-affected subjects have revealed several genes responsible for sperm flagellar defects. For example, *AK7* (MIM: 615364), *AKAP4* (MIM: 300185), *ARMC2*, *CFAP43* (MIM: 617558), *CFAP44* (MIM: 617559), *CFAP69* (MIM: 617949), *DNAH1* (MIM: 603332), *FSIP2* (MIM: 618153), *QRICH2* (MIM: 618304), and *WDR66* (also known as *CFAP251*; MIM: 618146).[12–26] However, the known MMAF-associated genes only account for approximately 60% of human MMAF cases. These findings indicate both that MMAF has a strong genetic heterogeneity and that, potentially, unknown genes involved in human MMAF exist.

[1]Obstetrics and Gynecology Hospital, NHC Key Laboratory of Reproduction Regulation (Shanghai Institute of Planned Parenthood Research), State Key Laboratory of Genetic Engineering at School of Life Sciences, Fudan University, Shanghai 200011, China; [2]Shanghai Key Laboratory of Female Reproductive Endocrine Related Diseases, Shanghai 200011, China; [3]State Key Laboratory of Reproductive Medicine, Center for Global Health, School of Public Health, Nanjing Medical University, Nanjing 211116, China; [4]Reproductive Medicine Center, Department of Obstetrics and Gynecology, the First Affiliated Hospital of Anhui Medical University, Hefei 230022, China; [5]Anhui Province Key Laboratory of Reproductive Health and Genetics, Anhui Medical University, Hefei 230022, China; [6]Anhui Provincial Engineering Technology Research Center for Biopreservation and Artificial Organs, Hefei 230022, China; [7]State Key Laboratory of Reproductive Medicine, the Affiliated Suzhou Hospital of Nanjing Medical University, Suzhou 215002, China; [8]Suzhou Municipal Hospital, Suzhou 215002, China; [9]Polyclinique les Jasmins, Centre d'Aide Médicale à la Procréation, Centre Urbain Nord, 1003 Tunis, Tunisia; [10]Genetic Epigenetic and Therapies of Infertility, Institute for Advanced Biosciences, Institut National de la Santé et de la Recherche Médicale U1209, Centre National de la Recherche Scientifique UMR 5309, Université Grenoble Alpes, Grenoble 38000, France; [11]Centre Hospitalier Universitaire de Grenoble, UM GI-DPI, Grenoble 38000, France; [12]Centre Hospitalier Universitaire de Grenoble, UM de Génétique Chromosomique, Grenoble 38000, France; [13]Department of Gynecology and Obstetrics, the Second Affiliated Hospital of Anhui Medical University, Hefei 230601, China
[14]These authors contributed equally to this work
[15]These authors contributed equally to this work
*Correspondence: caoyunxia6@126.com (Y.C.), zhangfeng@fudan.edu.cn (F.Z.)
https://doi.org/10.1016/j.ajhg.2019.02.020.

In this study, 65 unrelated Han Chinese men with MMAF were enrolled from the First Affiliated Hospital of Anhui Medical University and the Affiliated Suzhou Hospital of Nanjing Medical University in China. All 65 men presented with primary infertility, and none had obvious primary-ciliary-dyskinesia-related symptoms, such as bronchitis, sinusitis, otitis media, and pneumonia. Nine individuals were from consanguineous families. The cytogenetic karyotype analysis was performed in all of these cases, and it indicated normal male chromosomal karyotypes (46; XY) and no large-scale deletions in the human Y chromosome. This study was approved by the institutional review boards at Fudan University, the First Affiliated Hospital of Anhui Medical University, and the Affiliated Suzhou Hospital of Nanjing Medical University. Informed consent was obtained from each individual.

To investigate the unknown genetic factors involved in human MMAF, we carried out whole-exome sequencing (WES) and bioinformatic analyses on all 65 MMAF-affected men (see Supplemental Material and Methods). Intriguingly, bi-allelic mutations of *TTC21A* (tetratricopeptide repeat domain 21A, also known as *IFT139A*; MIM: 611430) were identified in one consanguineous family and two simplex individuals (Figure 1 and Table 1) who do not have bi-allelic pathogenic mutations in any known MMAF-associated genes. All the *TTC21A* mutations in MMAF-affected, Chinese men and their family members were verified by Sanger sequencing (Figure 1 and Table S1). TTC21A contains several tetratricopeptide repeat (TPR) domains that frequently exist in IFT proteins and seem important for ciliary function.[27,28] Notably, *TTC21A* is highly and specifically expressed in the human testis according to the databases of the Encyclopedia of DNA Elements (ENCODE), the Functional Annotation of the Mammalian Genome (FANTOM), and the Genotype-Tissue Expression (GTEx) project.

In the consanguineous family A004, a homozygous splice-site *TTC21A* mutation, c.716+1G>A, that alters a consensus splice donor site in intron 6 was identified in proband IV-1 (Figure 1A). To further investigate the consequence of splicing, we carried out reverse-transcription PCR (RT-PCR) and cDNA sequencing (Figure S1 and Table S2). The RT-PCR product obtained from proband A004 IV-1 was longer than that of a control male subject (Figure S1A). Sanger sequencing revealed a 1 bp substitution (c.716+1G>A) at the splice donor site and partial retention of intron 6 (Figure S1B). Explaining this aberration, the utilization of a downstream, cryptic splice donor site in intron 6 instead of the normal splice donor site leads to an immediate premature stop codon (p.Ile240*; Figure S1C).

In family A015, a stop-gain mutation, c.2329C>T (p.Gln777*), and a missense mutation, c.341A>G (p.Tyr114Cys), of *TTC21A* were identified in proband II-1 (Figure 1B). Notably, this missense mutation was predicted to be potentially deleterious by all three bioinformatic tools: SIFT, PolyPhen-2, and MutationTaster (Table 1). The variant p.Tyr114Cys was located at a conserved, cilia-related TPR domain of the TTC21A protein (Figure 1D). The bi-allelic mutations in subject A015 II-1 were confirmed to be inherited from parental heterozygous carriers. In family S022, proband II-1 was homozygous for the *TTC21A* stop-gain mutation c.2563del (p.Val855*) (Figure 1C).

To further estimate the allele frequencies of these candidate pathogenic mutations in *TTC21A*, we investigated 968 Han Chinese control individuals and the thousands of individuals archived in the 1000 Genomes Project and ExAC databases (Table 1). Our Han Chinese controls consisted of 300 healthy individuals and 668 individuals affected by non-reproductive disorders. The *TTC21A* missense mutation in subject A015 II-1 was extremely rare in the human population datasets (the allele frequency in East Asians of the ExAC database is 1.2×10^{-4}), and it was absent from the 968 Han Chinese individuals of the control group (Table 1). The other three *TTC21A* mutations in the MMAF-affected, Chinese individuals in this study were absent from the human population datasets (Table 1). These observations are consistent with the autosomal-recessive inheritance of MMAF pathogenesis.

In addition, WES and data analyses were also performed on an additional cohort of 167 men with MMAF. In this cohort, 83 individuals who originated from North Africa were enrolled from the Clinique des Jasmin in Tunis. 52 individuals with a Middle Eastern origin (Iran) were treated in Tehran at the Royan Institute. 32 individuals were recruited in France: 25 at the Cochin Institute, 3 in Rouen, 2 in Grenoble, and 1 in Lille and Caen. All of these affected individuals had primary infertility with a typical MMAF phenotype. The details of the cohort and of the performed analysis were previously reported.[25] Interestingly, a homozygous variant (c.3116+5G>T; Figure S2A) close to the *TTC21A* exon 23 splice donor site was identified in two unrelated Tunisian men (F001 and F002) from this cohort. This variant was also rare in the human population datasets and had an allelic frequency of 0.00058 in the Genome Aggregation Database (gnomAD). The *TTC21A* c.3116+5G>T variant was predicted to affect splicing by the Human Splicing Finder. RT-PCR was performed on sperm mRNA extracted from these two Tunisian subjects (F001 and F002) and two control subjects. The presence of cDNA was validated in both the controls and subjects by successful amplification of a control gene (*PRM1*). Amplification of *TTC21A* cDNA yielded a good signal in controls, but no amplification was obtained from the two *TTC21A*-mutated subjects, suggesting mRNA decay in these two subjects and thus validating the deleterious effect of variant c.3116+5G>T (Table S3 and Figure S2B).

The detailed phenotypes of the three Chinese, *TTC21A*-mutated men were examined through semen analysis and light microscopy (see Supplemental Material and Methods). Notably, the spermatozoa of subjects A004 IV-1 and S022 II-1 presented with very low motility and no progressive motility (Table 2). Severe abnormalities in

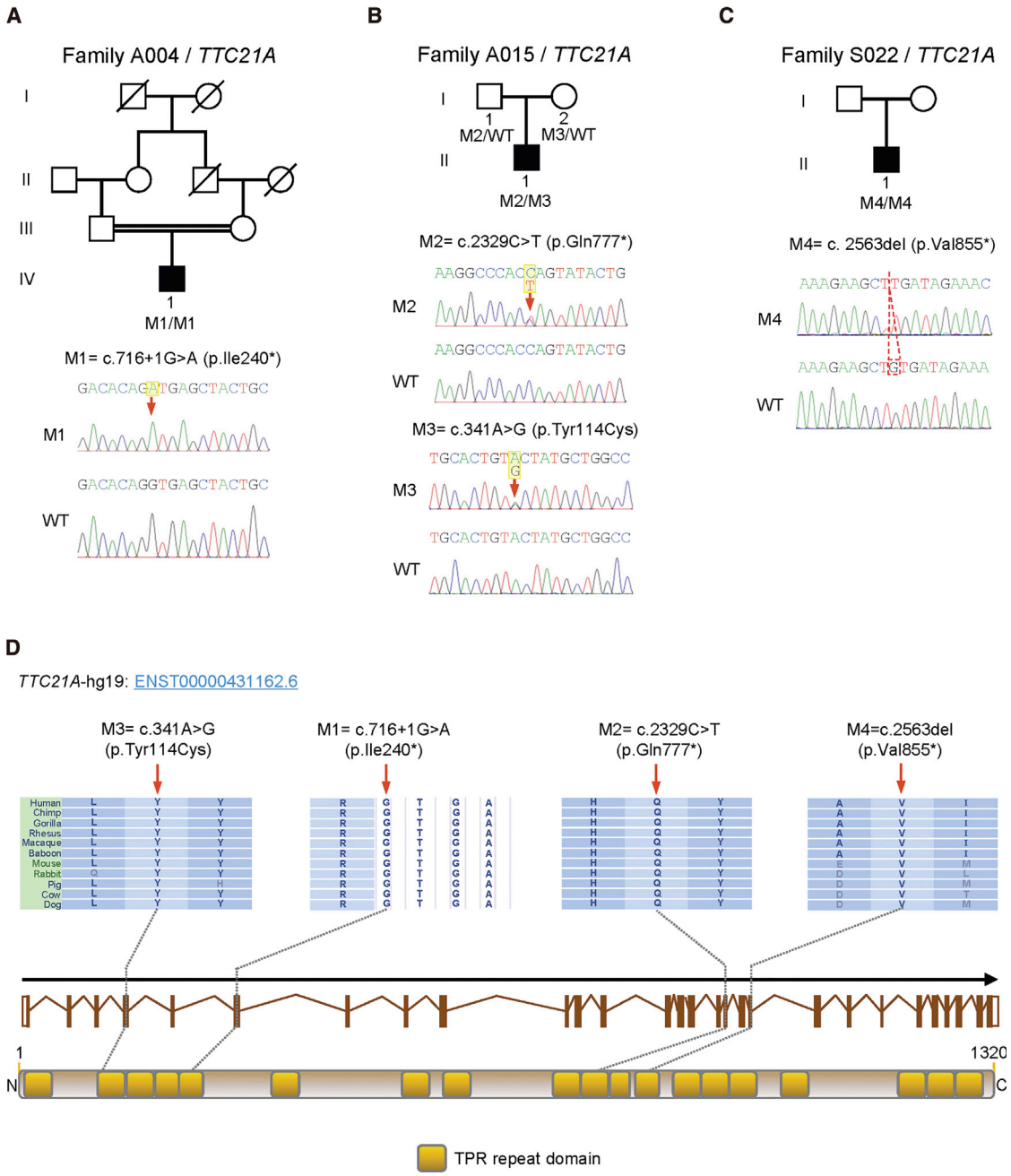

Figure 1. Bi-allelic *TTC21A* Mutations Identified in Chinese Men with MMAF-Associated Asthenoteratospermia

(A) A splice-site mutation, c.716+1G>A, of *TTC21A* was identified in the consanguineous family A004. The proband (IV-1) was homozygous for this mutation. The amino acid alteration was predicted according to the verified alteration of cDNA.

(B) Compound heterozygous mutations of *TTC21A* were identified in the proband (II-1) from family A015. The bi-allelic mutations were confirmed to be inherited from his parental, heterozygous carriers.

(C) A 1 bp deletion of c.2563del resulted in a *TTC21A* nonsense mutation in family S022. The proband (II-1) was homozygous for this mutation.

(D) These four *TTC21A* mutations (M1–M4) are located at the conserved sites in TPR domains.

Yellow squares stand for TPR repeat domains as described by the Uniprot server. All mutations were verified by Sanger sequencing. The mutation positions are indicated by red arrows and a dashed box. Mutations are annotated in accordance with the HGVS's recommendations. Abbreviations are as follows: WT = wild-type.

sperm motility were also observed in subject A015 II-1. No obvious reductions in semen volume and sperm concentration were observed in the *TTC21A*-mutated men according to the standard of the World Health Organization (WHO) guidelines.

Semen samples were stained according to the modified Papanicolaou staining protocol for morphological evaluation. At least 200 spermatozoa were examined under a light microscope (Figures 2A–E). All three Chinese men with bi-allelic *TTC21A* mutations consistently presented

Table 1. Bi-allelic *TTC21A* Mutations Identified in Chinese Men with Asthenoteratospermia

	Subject			
	A004 IV-1	A015 II-1		S022 II-1
Gene	**TTC21A**	**TTC21A**	**TTC21A**	**TTC21A**
DNA change[a]	c.716+1G>A (homozygous)	c.341A>G (allele 1)	c.2329C>T (allele 2)	c.2563del (homozygous)
Amino acid alteration[b]	p.Ile240*	p.Tyr114Cys	p.Gln777*	p.Val855*
Mutation type	splice site	missense	nonsense	nonsense
Allele Frequency in Human Populations				
East Asians in ExAC	0	1.2×10^{-4}	0	0
Han Chinese in 1000 Genomes Project	0	0	0	0
Han Chinese controls[c]	0	0	0	0
Conservation[d]				
PhyloP	5.292	4.669	0.481	2.439
PhastCons	1.000	1.000	1.000	0.116
Functional Prediction				
SIFT	N/A	damaging	N/A	N/A
PolyPhen-2	N/A	probably damaging	N/A	N/A
MutationTaster	N/A	disease causing	disease causing	N/A

Abbreviations are as follows: N/A = not applicable.
[a]The accession number of human *TTC21A* is GenBank: NM_145755.2.
[b]Full-length TTC21A has 1,320 amino acids.
[c]The Han Chinese controls consist of 300 fertile individuals and 668 individuals affected by non-reproductive disorders.
[d]The PhastCons value is close to 1 when a nucleotide is conserved, and the predicted conserved sites are assigned positive scores by PhyloP.

with sperm neck defects, such as abnormal and/or broken necks (Table 2). Two major categories of sperm morphological abnormalities were investigated: abnormal head-tail conjunction and abnormal flagella (Table 2). One spermatozoon might present morphological abnormalities simultaneously in the sperm neck and flagellum. There were five sub-categories of abnormal flagella: (1) short flagella, (2) absent flagella, (3) coiled flagella, (4) angulation of flagella, and (5) irregular caliber.[13] Each spermatozoon was classified to only one morphological sub-category of abnormal flagella according to its major flagellar abnormality.[29] Remarkably, no normal spermatozoa were apparent in any of the *TTC21A*-mutated men. Abnormal necks and short flagella were the most frequently observed defects in these cases (Table 2).

We conducted transmission electron microscopy (TEM) analyses to further investigate the ultra-structures of spermatozoa in the men with bi-allelic *TTC21A* mutations (see Supplemental Material and Methods). In contrast with the spermatozoa of the healthy male individual, spermatozoa of the *TTC21A*-mutated men had multiple ultra-structural abnormalities (Figures 2F–M). For example, cytoplasm residue and scattered and disorganized axonemal components were observed in the sperm necks and flagella (Figure 2G). Some cross sections showed absent or misplaced central-pair microtubules, absent or misplaced peripheral microtubule doublets, or hyperplasia of the fibrous sheaths (Figures 2I, 2K, and 2M).

To further investigate the biological consequences of *TTC21A* mutations in MMAF-affected men and the roles of *TTC21A* in sperm flagellar formation, we employed CRISPR-Cas9 technology to generate C57BL/6 mutant mice harboring a *Ttc21a* frameshift mutation.[30,31] The single-guide RNA (sgRNA) that was used in this study was specifically designed against chr9:119958998–119959075 (GRCm38/mm10) according to the position of the *TTC21A* stop-gain variant p.Val855*, which is closer to the TTC21A C terminus and might permit the translation of a longer truncated protein than those that are expected from the other two stop-gain variants (p.Ile240* and p.Gln777*) of this study. All experiments involving mice were performed according to the guideline for the care and use of laboratory animals of the US National Institutes of Health. This study was approved by the animal ethics committee at the School of Life Science, Fudan University.

A frameshift mutation (c.2534del) was identified in the founder mouse, and the presence of the variant in offspring was confirmed by Sanger sequencing (the primer information is provided in Table S4). This *Ttc21a* mutation (p.Lys845Argfs*5) was predicted to cause premature translational termination (Figure S3). Real-time quantitative PCR (RT-qPCR) assays that used RNA from mouse testes were performed to compare the relative expression of *Ttc21a* transcripts between wild-type (WT) and *Ttc21a*-mutated ($Ttc21a^{mut/mut}$) male mice. The primer sequences and RT-qPCR conditions are indicated in Table S5. Notably,

Table 2. Semen Characteristics and Sperm Morphology in Chinese Men with Bi-allelic *TTC21A* Mutations

		Subject		
		A004 IV-1	A015 II-1	S022 II-1
Gene		*TTC21A*	*TTC21A*	*TTC21A*
Semen Parameters				
Semen volume (mL)		4.6	3.4	3.8
Sperm concentration (10^6/mL)		27.8	13.9	9.4
Motility (%)		0.8	6.7	1.0
Progressive motility (%)		0.0	1.7	0.0
Sperm Morphology				
Normal spermatozoa (%)		0.0	0.0	0.0
Abnormal head-tail conjunction	Abnormal neck (%)	46.5	23.0	45.9
	Absent head (%)	0.5	0.5	1.3
Abnormal flagella	Short flagella (%)	63.0	82.0	89.0
	Absent flagella (%)	23.5	0.5	9.4
	Coiled flagella (%)	1.5	5.0	1.4
	Angulation (%)	2.5	1.0	0.0
	Irregular caliber (%)	5.5	2.0	0.0

the relative mRNA expression level of *Ttc21a* in the mutated mice was significantly reduced by approximately 26% compared to that in WT mice ($p < 0.001$) (Figure S4). This indicates partial nonsense-mediated mRNA decay triggered by premature translational termination. The commercially available antibody anti-TTC21A (Abcam, UK), which targets the C terminus of human TTC21A, failed to react with mouse TTC21A.

Pubescent male mice with heterozygous and homozygous *Ttc21a* mutations were mated with WT females, and the numbers of pups per litter were counted to evaluate fertility. Compared with the litters of the WT male mice, litters of homozygous *Ttc21a*-mutated male mice ($Ttc21a^{mut/mut}$) were significantly smaller (Figure 3E). Notably, approximately 78% of $Ttc21a^{mut/mut}$ male mice were infertile. No obvious difference of reproductive phenotypes was observed between WT and heterozygous *Ttc21a*-mutated carriers ($Ttc21a^{+/mut}$), further suggesting the autosomal-recessive inheritance for *Ttc21a*-associated asthenoteratospermia.

The publicly available data from the mouse ENCODE transcriptome and FANTOM5 project indicate that the expression of *Ttc21a* is predominant in adult mouse testes. Thus, we carefully assessed semen characteristics, sperm morphology, and the sperm ultra-structure of the *Ttc21a* mutant male mice (see Supplemental Material and Methods). Notably, the motility and progressive motility of spermatozoa were significantly reduced in the $Ttc21a^{mut/mut}$ male mice (Table S6).

Semen samples from mice were stained with hematoxylin and eosin. Morphological abnormalities of spermatozoa of the $Ttc21a^{mut/mut}$ male mice included short, coiled flagella and/or tailless spermatozoa (abnormal head-tail conjunction) (Figures 3B–D). The numbers of morphologically abnormal spermatozoa in the $Ttc21a^{mut/mut}$ male mice were carefully counted (Table S6). As observed in humans, the most frequently observed abnormality in the $Ttc21a^{mut/mut}$ male mice was abnormal head-tail conjunction in spermatozoa (Table S6).

TEM observations were also performed on the spermatozoa of the testes and the cauda epididymes from the $Ttc21a^{mut/mut}$ male mice, revealing the structural abnormalities of the connecting piece during spermiogenesis and multiple structural defects of the flagella (Figures 4 and S5). In round spermatids of the $Ttc21a^{mut/mut}$ mice, the Golgi apparatuses were forming acrosomes (Figures 4E and 4I), and the proximal centrioles were implanted normally into nuclear fossa (Figures 4F and 4J). During nuclear condensation and the late elongated stage, the connecting pieces were not formed or maintained successfully in spermatids of the $Ttc21a^{mut/mut}$ mice (Figures 4G, 4H, 4K, and 4L). The segmented columns and annulus were scattered. The mid-piece could not be formed without being surrounded by the mitochondria and having the annulus relocated, leading to an abnormal junction between the nucleus and the axoneme. These observations were consistent with the morphological abnormality of head-tail decapitation observed under light microscopy (Figure 3D). Additional axonemal structure abnormalities such as abnormal bulges, extra peripheral microtubule doublets, lack of central-pair microtubules, absent dynein arms, and abnormal arrangement of the nine peripheral microtubule doublets were also frequent (Figure S5).

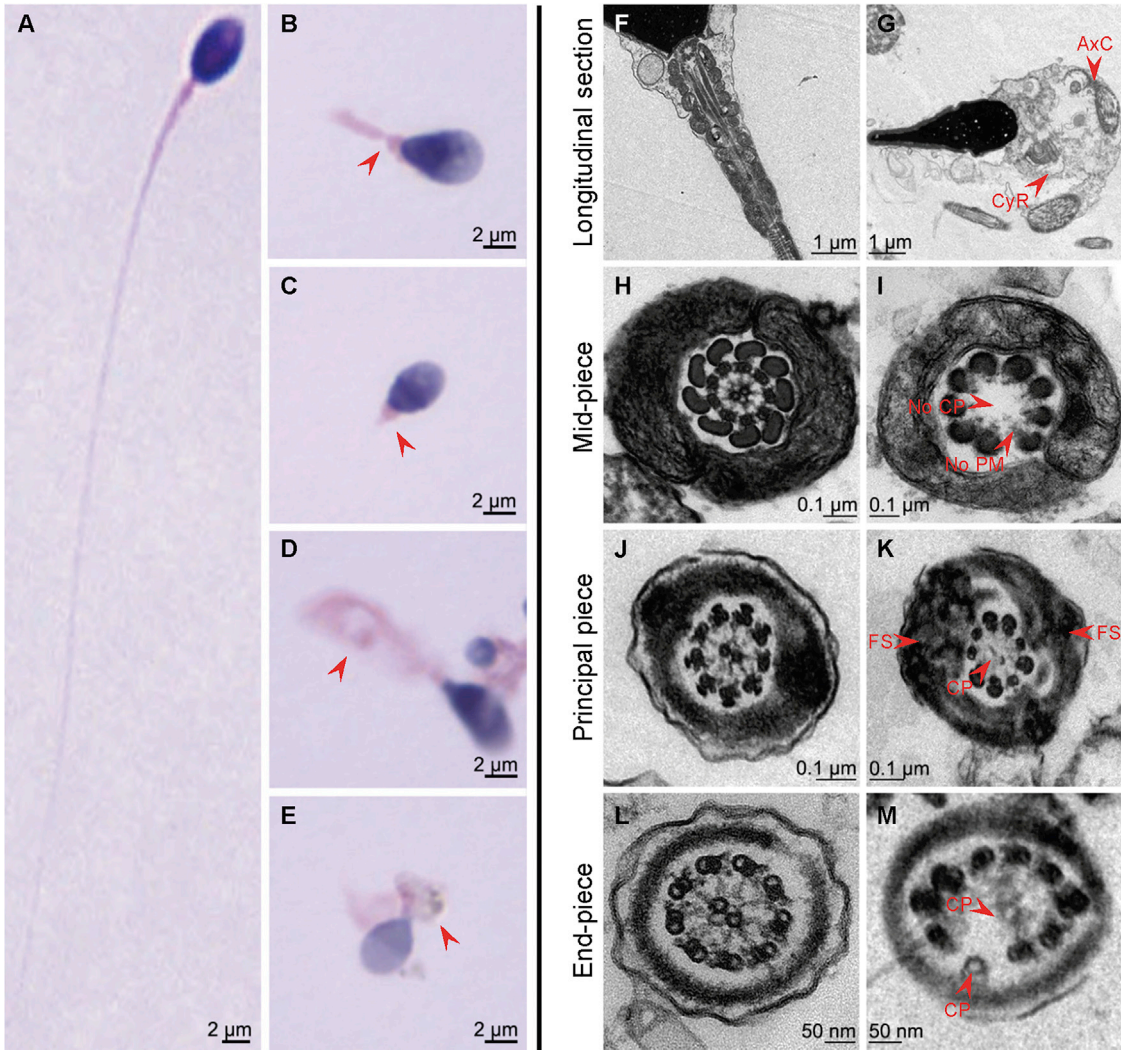

Figure 2. Sperm Morphology and Ultra-Structures

(A) Normal morphology of a spermatozoon from a healthy control man.

(B–E) Most spermatozoa of A015 II-1 presented with multiple morphological abnormalities (red arrows), such as abnormal sperm necks, abnormal flagella (e.g., absent, coiled, irregular-caliber, or short flagella), and cytoplasm residue.

(F) The longitudinal section of a normal spermatozoon from a healthy control man showed regular axonemal structures that had a normal connecting piece and a mitochondrial sheath in the mid-piece of the sperm flagellum.

(G) In A015 II-1, most spermatozoa presented cytoplasm residue and scattered and disorganized axonemal components in sperm necks and flagella.

(H, J, and L) The ultra-structures seen in a cross section of a normal spermatozoa from a healthy control man. The typical "9 + 2" microtubule structure is shown, consisting of nine peripheral microtubule doublets and the central pair of microtubules. The organized mitochondrial sheath, outer dense fibrous sheath, and fibrous sheath were all observed.

(I, K, and M) The cross sections in the spermatozoa from A015 II-1 revealed multiple ultra-structural abnormalities, such as missing or disordered central-pair microtubules, the absence or disorders of the nine peripheral microtubule doublets, or hyperplasia of the fibrous sheaths.

These sperm morphological abnormalities were confirmed in the other *TTC21A* mutant men.

Abbreviations are as follows: AxC = axonemal components; CyR = cytoplasm residue; CP = central-pair microtubules; FS = fibrous sheath; and PM = peripheral microtubule doublets.

As mentioned above, we identified six *TTC21A* mutant alleles in Chinese subjects with MMAF. The majority (5/6) of these *TTC21A* alleles contain stop-gain mutations (Figure S1). Furthermore, we compared the distributions of *TTC21A* loss-of-function (LoF) variants in the ExAC database and in this study (Table S7). Our observations ($p = 7.01 \times 10^{-7}$, two tailed Fisher's exact test) suggest that *TTC21A* LoF variants are associated with male infertility. Therefore, the MMAF phenotypes in these human subjects are preferentially explained by the bi-allelic mutations in *TTC21A*.

TTC21A encodes a member of the TPR family. Some proteins of the TPR family have been associated with ciliary function in non-human model organisms. For example, TTC10 (also known as IFT88) was previously reported to be involved in cilium biogenesis.[27] The mutations in

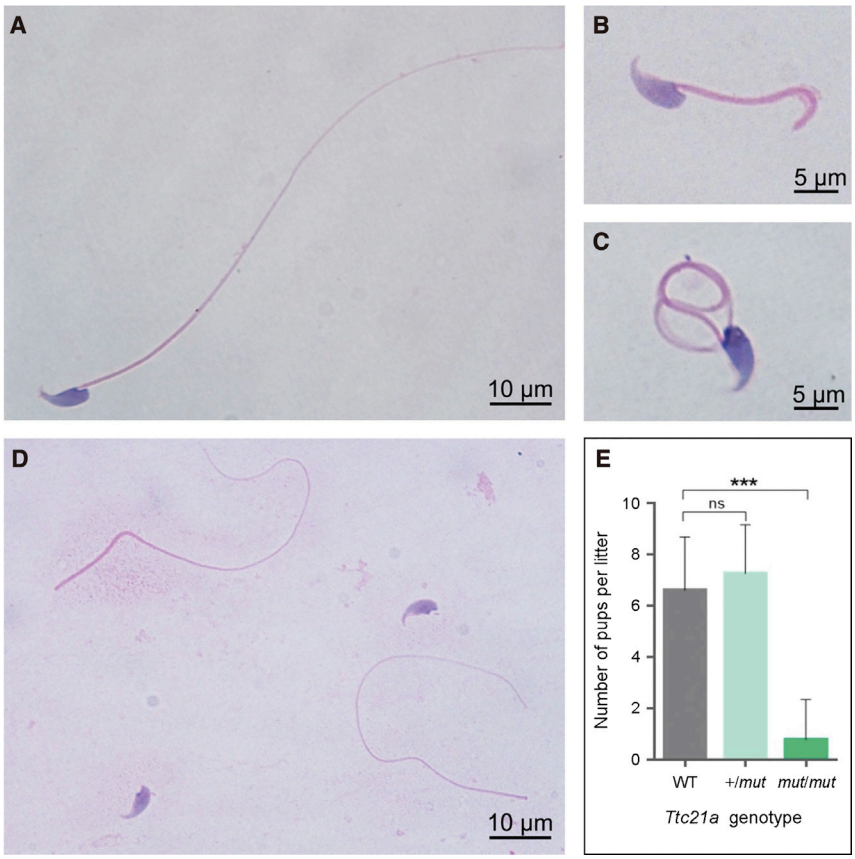

Figure 3. Sperm Morphology and Fertility of the *Ttc21a* Mutant Male Mice

(A) A spermatozoon from a wild-type (WT) male mouse.

(B–D) Multiple morphological abnormalities, including short, coiled flagella and/or tailless spermatozoa (abnormal head-tail conjunction), in the spermatozoa from the *Ttc21a* mutant ($Ttc21a^{mut/mut}$) male mice, were observed under light microscopy.

(E) Fertility of heterozygous ($Ttc21a^{+/mut}$) and homozygous ($Ttc21a^{mut/mut}$) male mice. Heterozygous and homozygous males were mated with WT females, and the numbers of pups per litter were counted. No significant difference in fertility was observed between the heterozygous carriers and the WT male mice. However, the litter sizes of homozygous mutated male mice were significantly reduced, and approximately 78% of these males were infertile. Error bars represent the standard error of the mean. *** $p < 0.001$ (Student's t test). Abbreviations are as follows: ns = no significance.

mouse *Ttc10* can cause polycystic kidneys.[27] Notably, some proteins of the TPR family (including TTC21A) are highly or preferentially expressed in the human testis according to the ENCODE, FANTOM, and GTEx databases. However, none of these TPR proteins had been directly linked to human male infertility. Our identification of biallelic *TTC21A* mutations in MMAF-affected men establishes the association between TRP proteins and human infertility.

TTC21A is also termed *IFT139A*. Although the molecular functions of TTC21A remains unclear, the data from functional protein association networks (STRING) interestingly indicated that the vast majority of predicted functional partners of both human TTC21A and mouse TTC21A were IFT components. The IFT particles contain two distinct protein complexes, A and B. As we mentioned above, IFT140 is a component of the IFT complex A, which is required for retrograde ciliary transport.[8] IFT20 and IFT52 are components of the IFT complex B, which also plays important roles in the development and maintenance of the cilia.[7,9] Therefore, we carried out co-immunoprecipitation (Co-IP) experiments using the antibodies (Proteintech) for these three IFT components (IFT140, IFT20, and IFT52), respectively. Total protein was extracted from semen samples of control human subjects. As shown in Figure S6, the interactions between TTC21A and these IFT components were revealed, suggesting that TTC21A is very likely an IFT component interacting with IFT proteins.

The assembly of the connecting piece, such as the segmented columns between the sperm head and tail, is organized by the proximal centrioles, whereas both flagellar axoneme and outer dense fibers (ODFs) originate from the distal centrioles.[32] The caudal ends of the nine segmented columns in the connecting piece fuse with the nine ODFs in the flagellar mid-piece during the late flagellar developmental stage.[32] Therefore, the assemblies of the connecting piece and flagellar axoneme seem to be independent of each other. However, previous studies in mouse *Spata6* strongly indicated that these two processes are, in fact, interrelated.[33] *Spata6* encodes a protein involved in myosin-based microfilament transport. This protein is required for the formation of the segmented columns and capitulum (parts essential for linking the developing flagellum to the head during late spermiogenesis), and its expression is restricted to the segmented columns and capitulum.[33] Intriguingly, TEM analysis of the *Spata6*-knockout mice evidenced malformations of both the segmented columns and of the axoneme;[33] these findings are quite similar to the observations made regarding the $Ttc21a^{mut/mut}$ mice of our study.

TTC21B (MIM: 612014), the paralog of *TTC21A*, encodes an intraflagellar transport-A component protein. The TTC21A and TTC21B proteins are approximately 50% identical in amino acid sequences and have similar TRP domains. Mutations in *TTC21B* were reported to be associated with various ciliopathies, but the *TTC21B* mutations were not described to induce male infertility.[34,35] According to the expression data from the Human Protein Atlas, *TTC21B* has ubiquitous expression in various tissues, including male tissues and female tissues,

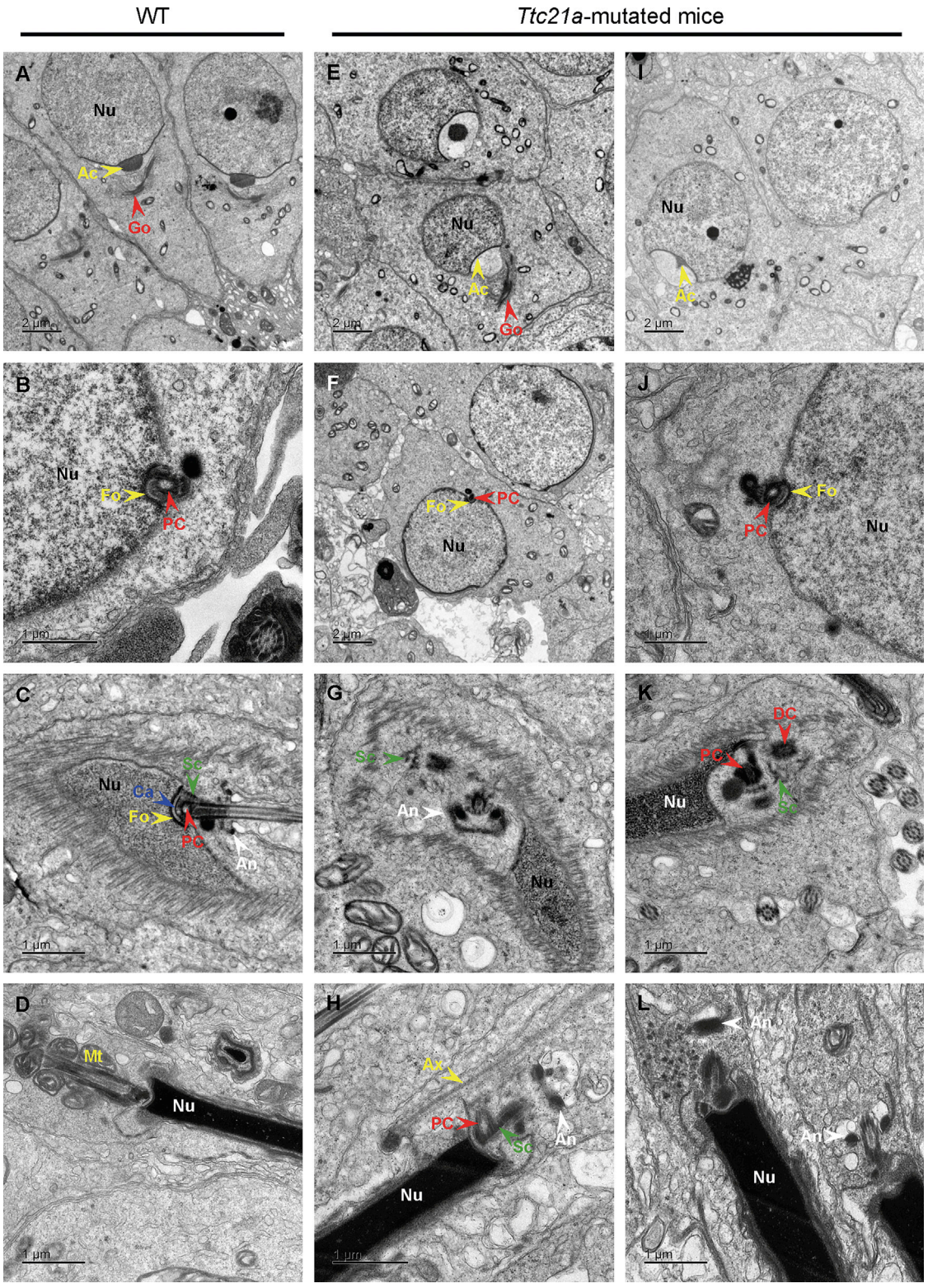

Figure 4. TEM Analyses of Testes from the *Ttc21a* Mutant Male Mice Reveal Structural Defects of the Connecting Piece During Spermiogenesis

(A–D) Representative ultra-structures of testicular spermatids from wild-type (WT) male mice during spermiogenesis. Golgi apparatuses were forming acrosomes (A), and the proximal centriole was transplanted into the nuclear fossa (B) in round spermatids. The connecting piece was formed by the assembly of the capitulum, proximal centriole, and segmented columns, and it was attached to the basal plates at the implantation fossa during nuclear condensation (C). In the late, elongated spermatid, the axoneme was surrounded by mitochondria and the forming mid-piece (D).

(legend continued on next page)

whereas the expression of *TTC21A* is high and specific to the testes. Moreover, the immunohistochemical signal of TTC21B can be detected in both cells of the seminiferous ducts and in Leydig cells. Specific TTC21A staining (Figure S7) is detected in preleptotene spermatocytes, pachytene spermatocytes, round spermatids, and elongated spermatids. In addition, our ultrastructural analyses of testes from the *Ttc21a*$^{mut/mut}$ male mice revealed some severe abnormalities of the connecting piece during nuclear condensation and the late elongated stage. The differential expressions between human *TTC21A* and *TTC21B*, together with our experimental observations made with TEM, strongly suggest that *TTC21A* has specific IFT functions in spermatogenesis.

In summary, our findings from both human subjects and the mouse model demonstrate that bi-allelic mutations in *TTC21A* can induce asthenoteratospermia characterized by reduced sperm motility and multiple sperm malformations. The *TTC21A*-associated morphological abnormalities affect sperm flagella and head-tail conjunction. The detailed molecular contributions of TTC21A to sperm flagellar formation and intraflagellar transport need to be further investigated in future studies. Our findings also suggest that other TPR-related genes or IFT transport genes could be involved in human asthenoteratospermia and other related ciliopathies.[36,37]

Supplemental Data

Supplemental Data can be found online at https://doi.org/10.1016/j.ajhg.2019.02.020.

Acknowledgments

We would like to thank the Center of Cryo-Electron Microscopy at Zhejiang University for technical support. This work was supported by the National Natural Science Foundation of China (31625015 and 31521003), the Foundation of the Department of Science and Technology of Anhui Province (2017070802D150), the Foundation of the Education Department of Anhui Province (KJ2016A370), the Shanghai Medical Center of Key Programs for Female Reproductive Diseases (2017ZZ01016), and the Shanghai Municipal Science and Technology Major Project (2017SHZDZX01).

Declaration of Interests

The authors declare no competing interests.

Received: October 10, 2018
Accepted: February 15, 2019
Published: March 28, 2019

Web Resources

1000 Genomes Project, http://www.internationalgenome.org
ENCODE, https://www.encodeproject.org
ExAC Browser, http://exac.broadinstitute.org
FANTOM, http://fantom.gsc.riken.jp
gnomAD, https://gnomad.broadinstitute.org
GTEx, http://www.gtexportal.org/home/
Human Protein Atlas, https://www.proteinatlas.org
Human Splicing Finder, http://www.umd.be/HSF3/
OMIM, http://www.omim.org
PolyPhen-2, http://genetics.bwh.harvard.edu/pph2/
SIFT, http://sift.jcvi.org
STRING, https://string-db.org
UCSC Genome Browser, http://genome.ucsc.edu
UniProt, https://www.uniprot.org

References

1. Inhorn, M.C., and Patrizio, P. (2015). Infertility around the globe: New thinking on gender, reproductive technologies and global movements in the 21st century. Hum. Reprod. Update *21*, 411–426.
2. Coutton, C., Escoffier, J., Martinez, G., Arnoult, C., and Ray, P.F. (2015). Teratozoospermia: Spotlight on the main genetic actors in the human. Hum. Reprod. Update *21*, 455–485.
3. Pedersen, L.B., and Rosenbaum, J.L. (2008). Intraflagellar transport (IFT) role in ciliary assembly, resorption and signalling. Curr. Top. Dev. Biol. *85*, 23–61.
4. Buisson, J., Chenouard, N., Lagache, T., Blisnick, T., Olivo-Marin, J.C., and Bastin, P. (2013). Intraflagellar transport proteins cycle between the flagellum and its base. J. Cell Sci. *126*, 327–338.
5. Piperno, G., and Mead, K. (1997). Transport of a novel complex in the cytoplasmic matrix of Chlamydomonas flagella. Proc. Natl. Acad. Sci. USA *94*, 4457–4462.
6. Ishikawa, H., and Marshall, W.F. (2011). Ciliogenesis: Building the cell's antenna. Nat. Rev. Mol. Cell Biol. *12*, 222–234.
7. Deane, J.A., Cole, D.G., Seeley, E.S., Diener, D.R., and Rosenbaum, J.L. (2001). Localization of intraflagellar transport protein IFT52 identifies basal body transitional fibers as the docking site for IFT particles. Curr. Biol. *11*, 1586–1590.
8. Zhang, Y., Liu, H., Li, W., Zhang, Z., Zhang, S., Teves, M.E., Stevens, C., Foster, J.A., Campbell, G.E., Windle, J.J., et al. (2018). Intraflagellar transporter protein 140 (IFT140), a component of IFT-A complex, is essential for male fertility and spermiogenesis in mice. Cytoskeleton (Hoboken) *75*, 70–84.

(E–L) Ultra-structures of testicular spermatids from the *Ttc21a*$^{mut/mut}$ male mice during spermiogenesis. No obvious abnormality was observed in the early deformation stage of the round spermatid (E–J). However, during nuclear condensation and the late deformation stage, abnormal formations of the connecting pieces were observed. The structures indicated by green arrows were columnar, which was consistent with the previously reported structural characteristics of segmented columns.[33] Several similar columnar structures appeared nearby. These columnar structures and annulus were scattered (G and K). The mid-pieces could not be formed without being surrounded by mitochondria and without relocation of the annulus (H and L). The misalignment between nucleus and axoneme was observed as well (H and L).
Abbreviations are as follows: Ac = acrosome; An = annulus; Ax = axoneme; Ca = capitilum; Dc = distal centriole; Fo = fossa; Go = Golgi apparatus; Mt = mitochondrion; Nu = nucleus; Pc = proximal centriole; and Sc = segmented column.

9. Zhang, Z., Li, W., Zhang, Y., Zhang, L., Teves, M.E., Liu, H., Strauss, J.F., 3rd, Pazour, G.J., Foster, J.A., Hess, R.A., and Zhang, Z. (2016). Intraflagellar transport protein IFT20 is essential for male fertility and spermiogenesis in mice. Mol. Biol. Cell *27*, 3705–3716.
10. Liu, H., Li, W., Zhang, Y., Zhang, Z., Shang, X., Zhang, L., Zhang, S., Li, Y., Somoza, A.V., Delpi, B., et al. (2017). IFT25, an intraflagellar transporter protein dispensable for ciliogenesis in somatic cells, is essential for sperm flagella formation. Biol. Reprod. *96*, 993–1006.
11. Zhang, Y., Liu, H., Li, W., Zhang, Z., Shang, X., Zhang, D., Li, Y., Zhang, S., Liu, J., Hess, R.A., et al. (2017). Intraflagellar transporter protein (IFT27), an IFT25 binding partner, is essential for male fertility and spermiogenesis in mice. Dev. Biol. *432*, 125–139.
12. Baccetti, B., Collodel, G., Estenoz, M., Manca, D., Moretti, E., and Piomboni, P. (2005). Gene deletions in an infertile man with sperm fibrous sheath dysplasia. Hum. Reprod. *20*, 2790–2794.
13. Ben Khelifa, M., Coutton, C., Zouari, R., Karaouzène, T., Rendu, J., Bidart, M., Yassine, S., Pierre, V., Delaroche, J., Hennebicq, S., et al. (2014). Mutations in DNAH1, which encodes an inner arm heavy chain dynein, lead to male infertility from multiple morphological abnormalities of the sperm flagella. Am. J. Hum. Genet. *94*, 95–104.
14. Tang, S., Wang, X., Li, W., Yang, X., Li, Z., Liu, W., Li, C., Zhu, Z., Wang, L., Wang, J., et al. (2017). Biallelic mutations in CFAP43 and CFAP44 cause male infertility with multiple morphological abnormalities of the sperm flagella. Am. J. Hum. Genet. *100*, 854–864.
15. Coutton, C., Vargas, A.S., Amiri-Yekta, A., Kherraf, Z.E., Ben Mustapha, S.F., Le Tanno, P., Wambergue-Legrand, C., Karaouzène, T., Martinez, G., Crouzy, S., et al. (2018). Mutations in CFAP43 and CFAP44 cause male infertility and flagellum defects in Trypanosoma and human. Nat. Commun. *9*, 686.
16. Sha, Y.W., Wang, X., Su, Z.Y., Mei, L.B., Ji, Z.Y., Bao, H., and Li, P. (2019). Patients with multiple morphological abnormalities of the sperm flagella harbouring CFAP44 or CFAP43 mutations have a good pregnancy outcome following intracytoplasmic sperm injection. Andrologia *51*, e13151.
17. Lorès, P., Coutton, C., El Khouri, E., Stouvenel, L., Givelet, M., Thomas, L., Rode, B., Schmitt, A., Louis, B., Sakheli, Z., et al. (2018). Homozygous missense mutation L673P in adenylate kinase 7 (AK7) leads to primary male infertility and multiple morphological anomalies of the flagella but not to primary ciliary dyskinesia. Hum. Mol. Genet. *27*, 1196–1211.
18. Dong, F.N., Amiri-Yekta, A., Martinez, G., Saut, A., Tek, J., Stouvenel, L., Lorès, P., Karaouzène, T., Thierry-Mieg, N., Satre, V., et al. (2018). Absence of CFAP69 causes male infertility due to multiple morphological abnormalities of the flagella in human and mouse. Am. J. Hum. Genet. *102*, 636–648.
19. He, X., Li, W., Wu, H., Lv, M., Liu, W., Liu, C., Zhu, F., Li, C., Fang, Y., Yang, C., et al. (2019). Novel homozygous *CFAP69* mutations in humans and mice cause severe asthenoteratospermia with multiple morphological abnormalities of the sperm flagella. J. Med. Genet. *56*, 96–103.
20. Kherraf, Z.E., Amiri-Yekta, A., Dacheux, D., Karaouzène, T., Coutton, C., Christou-Kent, M., Martinez, G., Landrein, N., Le Tanno, P., Fourati Ben Mustapha, S., et al. (2018). A homozygous ancestral SVA-insertion-mediated deletion in WDR66 induces multiple morphological abnormalities of the sperm flagellum and male infertility. Am. J. Hum. Genet. *103*, 400–412.
21. Auguste, Y., Delague, V., Desvignes, J.P., Longepied, G., Gnisci, A., Besnier, P., Levy, N., Beroud, C., Megarbane, A., Metzler-Guillemain, C., and Mitchell, M.J. (2018). Loss of calmodulin- and radial-spoke-associated complex protein CFAP251 leads to immotile spermatozoa lacking mitochondria and infertility in men. Am. J. Hum. Genet. *103*, 413–420.
22. Li, W., He, X., Yang, S., Liu, C., Wu, H., Liu, W., Lv, M., Tang, D., Tan, J., Tang, S., et al. (2019). Biallelic mutations of CFAP251 cause sperm flagellar defects and human male infertility. J. Hum. Genet. *64*, 49–54.
23. Martinez, G., Kherraf, Z.E., Zouari, R., Fourati Ben Mustapha, S., Saut, A., Pernet-Gallay, K., Bertrand, A., Bidart, M., Hograindleur, J.P., Amiri-Yekta, A., et al. (2018). Whole-exome sequencing identifies mutations in FSIP2 as a recurrent cause of multiple morphological abnormalities of the sperm flagella. Hum. Reprod. *33*, 1973–1984.
24. Liu, W., Wu, H., Wang, L., Yang, X., Liu, C., He, X., Li, W., Wang, J., Chen, Y., Wang, H., et al. (2018). Homozygous loss-of-function mutations in FSIP2 cause male infertility with asthenoteratospermia. J. Genet. Genomics *46*. S1673-8527(18)30204-2. https://doi.org/10.1016/j.jgg.2018.09.006.
25. Coutton, C., Martinez, G., Kherraf, Z.E., Amiri-Yekta, A., Boguenet, M., Saut, A., He, X., Zhang, F., Cristou-Kent, M., Escoffier, J., et al. (2019). Bi-allelic mutations in ARMC2 lead to severe astheno-teratozoospermia due to sperm flagellum malformations in humans and mice. Am. J. Hum. Genet. *104*, 331–340.
26. Shen, Y., Zhang, F., Li, F., Jiang, X., Yang, Y., Li, X., Li, W., Wang, X., Cheng, J., Liu, M., et al. (2019). Loss-of-function mutations in QRICH2 cause male infertility with multiple morphological abnormalities of the sperm flagella. Nat. Commun. *10*, 433.
27. Pazour, G.J., Dickert, B.L., Vucica, Y., Seeley, E.S., Rosenbaum, J.L., Witman, G.B., and Cole, D.G. (2000). Chlamydomonas IFT88 and its mouse homologue, polycystic kidney disease gene tg737, are required for assembly of cilia and flagella. J. Cell Biol. *151*, 709–718.
28. van Dam, T.J., Townsend, M.J., Turk, M., Schlessinger, A., Sali, A., Field, M.C., and Huynen, M.A. (2013). Evolution of modular intraflagellar transport from a coatomer-like progenitor. Proc. Natl. Acad. Sci. USA *110*, 6943–6948.
29. Yang, S.M., Li, H.B., Wang, J.X., Shi, Y.C., Cheng, H.B., Wang, W., Li, H., Hou, J.Q., and Wen, D.G. (2015). Morphological characteristics and initial genetic study of multiple morphological anomalies of the flagella in China. Asian J. Androl. *17*, 513–515.
30. Ran, F.A., Hsu, P.D., Wright, J., Agarwala, V., Scott, D.A., and Zhang, F. (2013). Genome engineering using the CRISPR-Cas9 system. Nat. Protoc. *8*, 2281–2308.
31. Abbasi, F., Miyata, H., and Ikawa, M. (2017). Revolutionizing male fertility factor research in mice by using the genome editing tool CRISPR/Cas9. Reprod. Med. Biol. *17*, 3–10.
32. Chemes, H.E. (2012). Sperm Centrioles and Their Dual Role in Flagellogenesis and Cell Cycle of the Zygote. In The Centrosome: Cell and Molecular Mechanisms of Functions and Dysfunctions in Disease, H. Schatten, ed. (Totowa, NJ: Humana Press), pp. 33–48.
33. Yuan, S., Stratton, C.J., Bao, J., Zheng, H., Bhetwal, B.P., Yanagimachi, R., and Yan, W. (2015). Spata6 is required for normal

assembly of the sperm connecting piece and tight head-tail conjunction. Proc. Natl. Acad. Sci. USA *112*, E430–E439.
34. Tran, P.V., Haycraft, C.J., Besschetnova, T.Y., Turbe-Doan, A., Stottmann, R.W., Herron, B.J., Chesebro, A.L., Qiu, H., Scherz, P.J., Shah, J.V., et al. (2008). THM1 negatively modulates mouse sonic hedgehog signal transduction and affects retrograde intraflagellar transport in cilia. Nat. Genet. *40*, 403–410.
35. Davis, E.E., Zhang, Q., Liu, Q., Diplas, B.H., Davey, L.M., Hartley, J., Stoetzel, C., Szymanska, K., Ramaswami, G., Logan, C.V., et al.; NISC Comparative Sequencing Program (2011). TTC21B contributes both causal and modifying alleles across the ciliopathy spectrum. Nat. Genet. *43*, 189–196.
36. Badano, J.L., Mitsuma, N., Beales, P.L., and Katsanis, N. (2006). The ciliopathies: An emerging class of human genetic disorders. Annu. Rev. Genomics Hum. Genet. *7*, 125–148.
37. Fliegauf, M., Benzing, T., and Omran, H. (2007). When cilia go bad: Cilia defects and ciliopathies. Nat. Rev. Mol. Cell Biol. *8*, 880–893.

The American Journal of Human Genetics, Volume *104*

Supplemental Data

Bi-allelic Mutations in *TTC21A* Induce Asthenoteratospermia in Humans and Mice

Wangjie Liu, Xiaojin He, Shenmin Yang, Raoudha Zouari, Jiaxiong Wang, Huan Wu, Zine-Eddine Kherraf, Chunyu Liu, Charles Coutton, Rui Zhao, Dongdong Tang, Shuyan Tang, Mingrong Lv, Youyan Fang, Weiyu Li, Hong Li, Jianyuan Zhao, Xue Wang, Shimin Zhao, Jingjing Zhang, Christophe Arnoult, Li Jin, Zhiguo Zhang, Pierre F. Ray, Yunxia Cao, and Feng Zhang

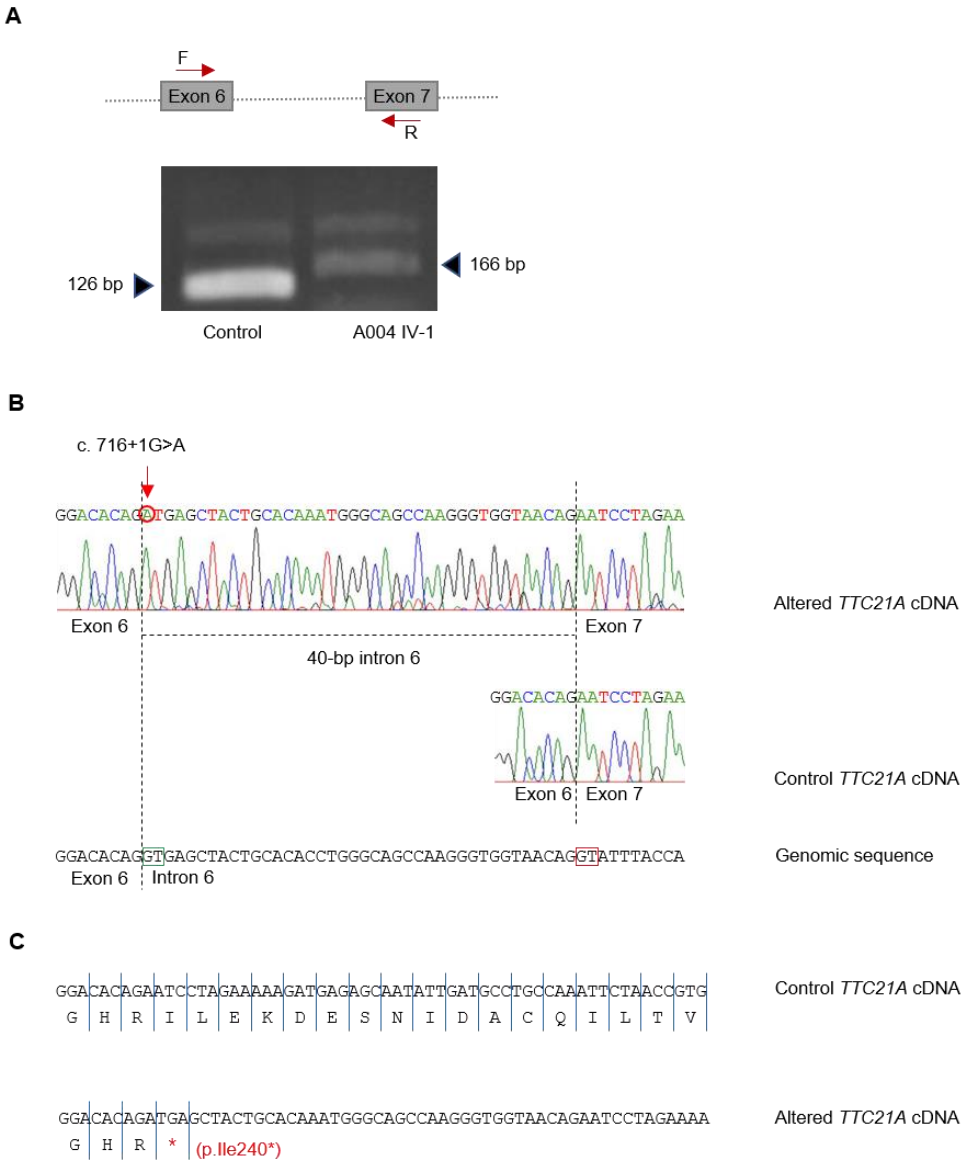

Figure S1. Splicing Alteration Caused by the *TTC21A* Splice-Site Mutation in Human Subject A004 IV-1.

(A) The forward and reverse primers were respectively designed in exons 6 and 7 of *TTC21A* for amplification and sequencing of cDNA. The RT-PCR product obtained from subject A004 IV-1 is longer than that from the control subject. (B) Sanger sequencing revealed a 1 bp substitution of c.716+1G>A (red arrow) at the splice donor site of intron 6. This splice-site mutation resulted in the partial retention of intron 6. The aberration can be explained by the utilization of a downstream cryptic splice donor site (red rectangle) in intron 6 instead of the normal splice donor site (green rectangle). (C) Immediate premature stop codon (p.Ile240*) was predicted according to the altered cDNA sequence of *TTC21A*.

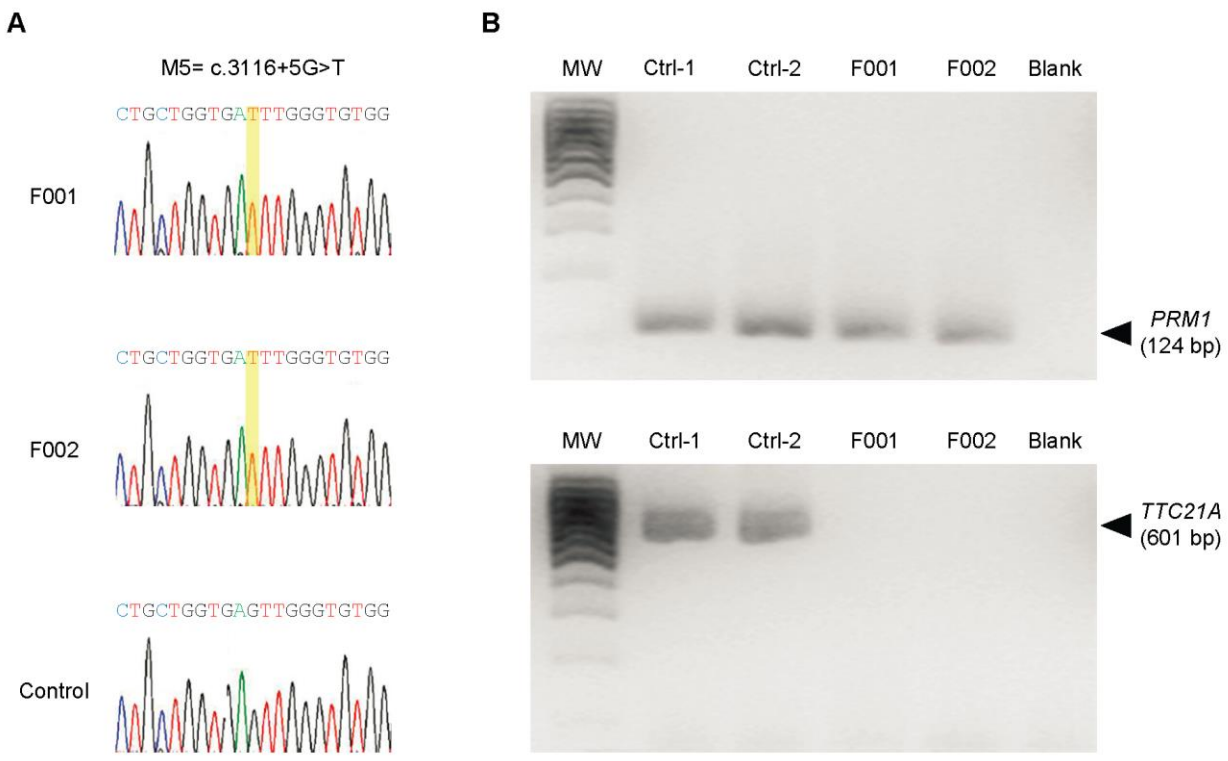

Figure S2. A Homozygous Splicing Mutation of *TTC21A* in Two Unrelated Tunisian Men with MMAF.

(A) The homozygous splicing mutation (c.3116+5G>T) of *TTC21A* was newly identified in two Tunisian men by WES and was further confirmed by Sanger sequencing. (B) To investigate potential deleterious effect of the splicing variant c.3116+5G>T, total RNA was extracted from sperm samples of these two *TTC21A*-mutated subjects (F001 and F002). The amplification of a cDNA sequence ranging from exons 21 to 26 yielded a normal band of 601 bp in control samples (Ctrl-1 and Ctrl-2) whereas no amplification was detected from sperm samples of two *TTC21A*-mutated subjects. *PRM1* was used as an internal control gene.

Figure S3. The Frameshift Mutation c.2534del Generated in the Mouse *Ttc21a*.
(A) A *Ttc21a* frameshift mutation c.2534del (*Ttc21a*^{mut}) was generated in mice using CRSIPR-Cas9 technology. The deleted nucleotide was shown by a red dash. (B) This frameshift mutation was predicted to cause premature translational termination (p.Lys845Argfs*5) of *Ttc21a*. The termination codon (red asterisk) was shown in the mutated cDNA.

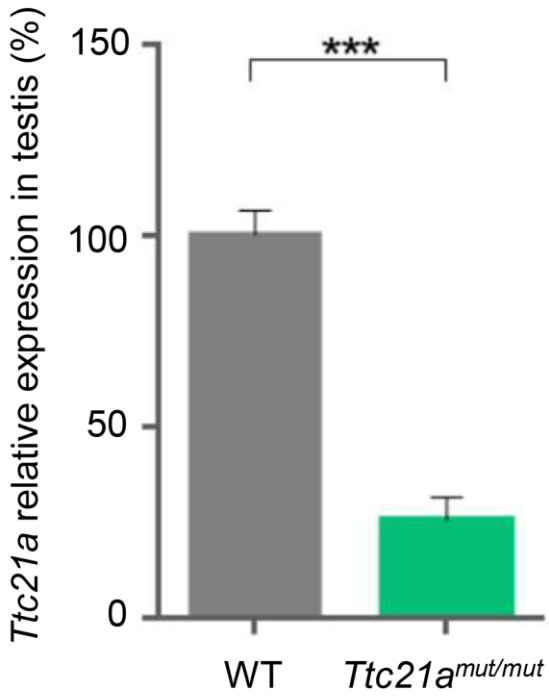

Figure S4. Expression Analysis of *Ttc21a* mRNA in the *Ttc21a*-Mutated Male Mice.
RT-qPCR assays showed that the mRNA level of *Ttc21a* in testes of the *Ttc21a*-mutated mice (*Ttc21a*$^{mut/mut}$) was reduced to approximately 26% of that in the wild-type (WT) mice. At least three testes were used for biological replicates. The internal control gene used for these assays was *Gapdh*. Each sample was assayed in triplicate for technical replicates. Error bars represent the standard error of the mean. *** $P < 0.001$ (Student's *t*-test).

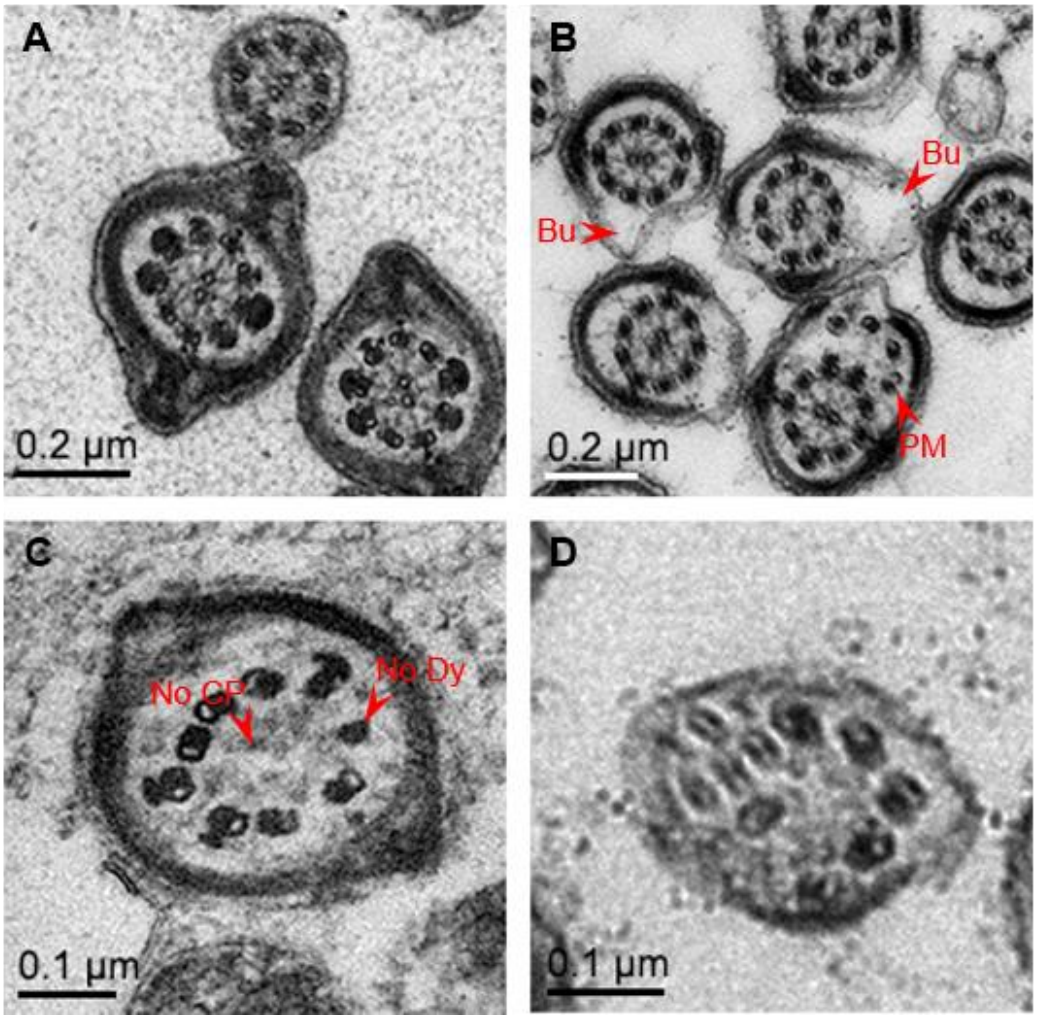

Figure S5. TEM Analyses of Spermatozoa from the *Ttc21a*-Mutated Male Mice Revealed Defects of the Flagella.

(A) The cross sections of normal spermatozoa from the WT male mice showed typical "9+2" microtubule structures. (B-D) Multiple structural abnormalities were observed in the sperm flagella of the *Ttc21a*-mutated male mice (*Ttc21a*$^{mut/mut}$). These structural abnormalities included abnormal bulges (Bu), extra peripheral microtubule doublets (PM), lacks of central-pair microtubules (CP), absent dynein arms (Dy), and abnormal arrangement of the nine peripheral microtubule doublets.

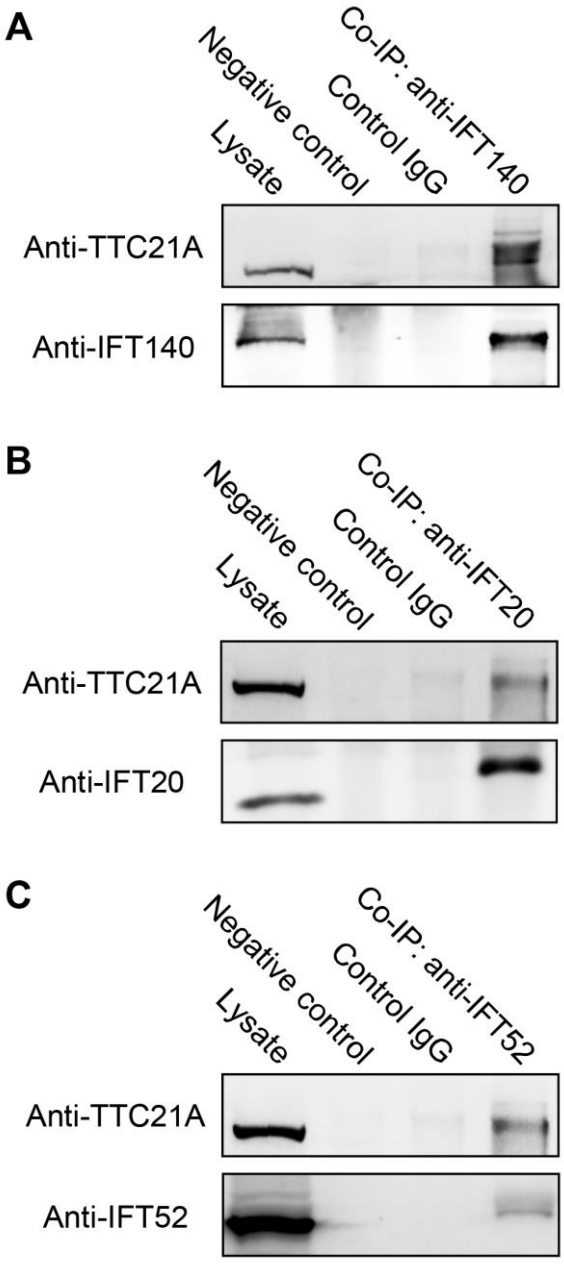

Figure S6. Co-Immunoprecipitation (Co-IP) Assays of Human Spermatozoa Revealed the Interactions between TTC21A and Known IFT Proteins.

Total protein was extracted from semen samples of human control subjects. Co-IP assays were respectively performed with the IFT antibodies (Proteintech, USA), including anti-IFT140 (A), anti-IFT20 (B) anti-IFT52 (C). Protein A agarose beads (EMD Millipore, USA) were used for enrichment. The negative control only contained protein A beads without any antibody. Lysate was also immunoprecipitated with normal rabbit IgG (Abcam, UK) as controls. Western blot experiments were performed using anti-TTC21A (Abcam, UK) and the corresponding IFT antibodies. The positive TTC21A signals were detected in lysate and Co-IP groups, suggesting the interactions between TTC21A and these known IFT proteins.

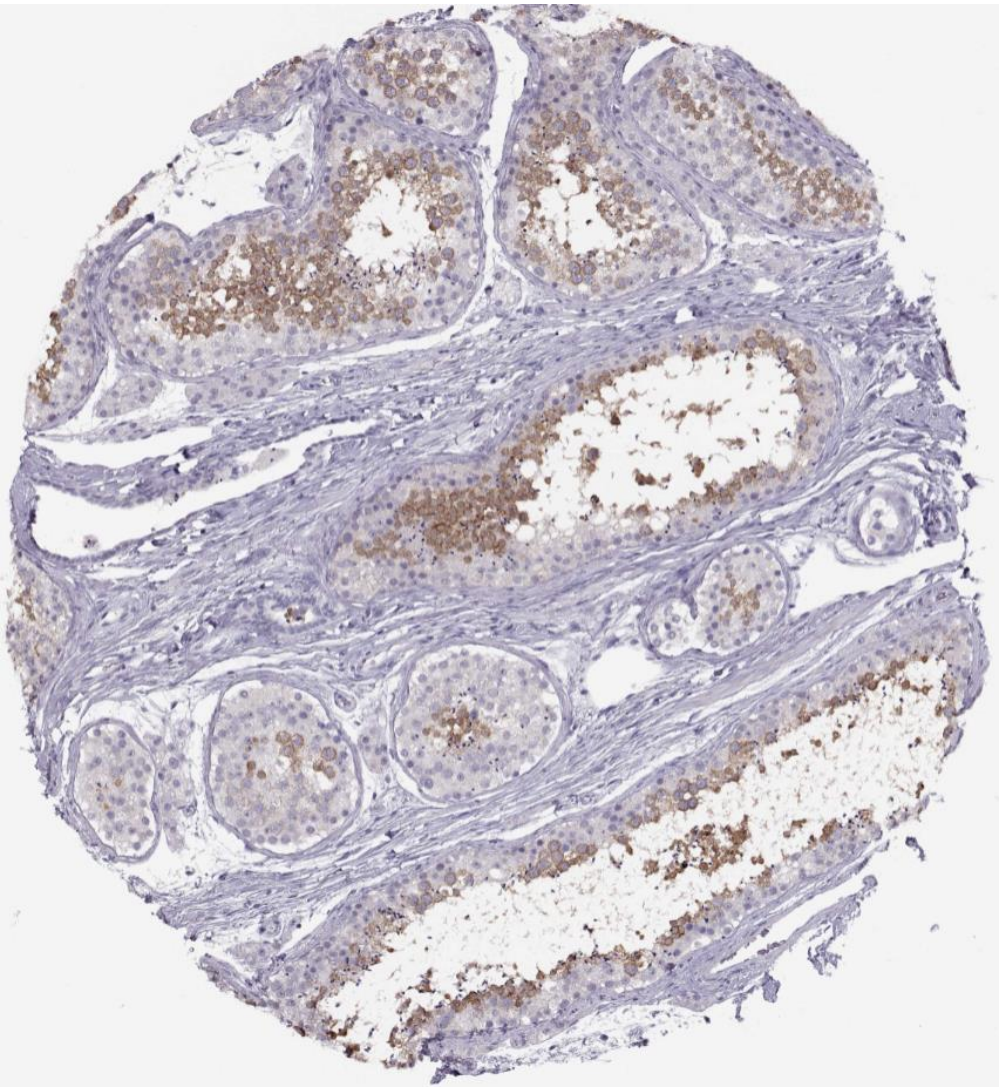

Figure S7. TTC21A is specifically expressed in the germ cell lineage.

The image of immunohistochemical staining in human testicular tissue is available from the Human Protein Atlas. Specific TTC21A staining is detected in preleptotene spermatocytes, pachytene spermatocytes, round spermatids, and elongated spermatids, suggesting that TTC21A may play an important role in spermatogenesis.

Web link: https://www.proteinatlas.org/ENSG00000168026-TTC21A/tissue/testis#img

Table S1. Primers Used for Amplification and Verification of the *TTC21A* Mutations

Primer Name	Primer Sequence (5'-3')	Tm
M1-F	CTTTTCACTTTAGGCTATGTTCTGGAGGGG	61 ℃
M1-R	GTGTACCATAACTGAATGAACCAGGACGGG	
M2-F	TGACCTCACATGGCCTTACCCTATC	61 ℃
M2-R	ATTCTAGTCTCATTCTCCTGCCAGT	
M3-F	TGGCCTAACTACAGAGATGGATGTG	60 ℃
M3-R	TCTTTAACTTCAGGAGCAGTTTGCC	
M4-F	GATCTTGTCAGAAAAACCAAGCCAA	60 ℃
M4-R	TGGTGCAAGCCATAGAAAATCTATC	

Table S2. Primers Used for Functional Investigations on the *TTC21A* Splice-Site Mutation c.716+1G>A

Primer Name	Primer Sequence (5'-3')	Tm
A004-cDNA-F	CTTTTCACTTTAGGCTATGTTCTGGAGGGG	61 ℃
A004-cDNA-R	GTGTACCATAACTGAATGAACCAGGACGGG	

Table S3. Primers Used for Functional Investigations on the *TTC21A* Splicing Mutation c.3116+5G>T

Primer Name	Primer Sequence (5'-3')	Product Size (bp)
PRM1-F1	TGACTCACAGCCCACAGAGT	124
PRM1-R1	CTGCGACAGCATCTGTACCT	
*TTC21A*_RT-F1	CGCTTCTGTGTTGATGGCTG	601
*TTC21A*_RT-R1	CTTCTCAGCCTGCGCTATCT	

Table S4. Primers Used for Mouse *Ttc21a* Genotyping

Primer Name	Primer Sequence (5'-3')	Tm
Ttc21a-F	ATTACTACGAGGCTGCCCAGAAGAT	61 ℃
Ttc21a-R	CAAAGGTGTAGACTGAGGGAGCAGA	

Table S5. Primers Used for RT-qPCR Analysis

Primer Name	Primer Sequence (5'-3')	Tm
Ttc21a-RT-F	GTGGGCCTAGAGAGGTACAG	60 ℃
Ttc21a-RT-R	GTGGGCCTAGAGAGGTACAG	
Gapdh-F	GTGGGCCTAGAGAGGTACAG	60 ℃
Gapdh-R	TGAAGGGGTCGTTGATGGC	

Table S6. Semen Characteristics, Sperm Morphology and Ultrastructural Abnormalities in the *Ttc21a*-Mutated Male Mice

	Wild-Type Male Mice [a]	*Ttc21a*$^{mut/mut}$ Male Mice [a]
Semen Parameters		
Semen count (10^6) [b]	6.5 (6.0-7.1)	6.4 (6.0-7.2)
Motility (%)	84 (78-90)	39 (0-86)
Progressive motility (%)	74 (62-87)	33 (0-79)
Sperm Morphology		
Normal spermatozoa (%)	83.3 (83.0-90.0)	26.7 (1.0-74.0)
Abnormal head-tail conjunction (%)	4.9 (3.0-10.0)	60.7 (16.5-92.5)
Short flagella (%)	1.0 (0.5-2)	10.5 (0.5-29.5)
Coiled flagella (%)	2.0 (1.5-2.0)	6.1 (2.0-14.5)
Angulation (%)	0 (0-0)	2.0 (0-4.5)
Irregular caliber (%)	0 (0-0)	0.3 (0-1.0)
Flagellar Ultrastructural Abnormalities [c]		
Abnormal principle pieces (%)	3.4 (2.4-5.2)	17.2 (5.0-27.3)
Abnormal end pieces (%)	2.3 (0.3-3.5)	32.6 (15.6-46.2)

[a] Values represent the mean (range).

[b] Per single epididymis.

[c] More than one hundred cross sections were analyzed.

Table S7. Distributions of the *TTC21A* Loss-of-Function (LoF) Alleles in Our Chinese MMAF Cohort and the Human Populations Archived by the ExAC Database

***TTC21A* Allele**	**Chinese MMAF**	**ExAC**	***P* Value ***
Allele numbers of LoF variants	5	148	7.01×10^{-7}
Allele numbers of non-LoF variants	125	122824	

* Two tailed Fisher's exact test

Supplemental Methods

Whole-Exome Sequencing and Bioinformatic Analysis

The DNeasy Blood and Tissue Kit (QIAGEN, Germany) was employed to extract genomic DNAs from peripheral blood samples of human subjects and their available parents. The whole human exome was enriched and constructed as a DNA library using the SureSelect^{XT} Human All Exon Kit (Agilent, USA). Next-generation sequencing was carried out on the HiSeq X-TEN platform (Illumina, USA). Sequencing reads were aligned to the human genome reference assembly (GRCh37/hg19) using the Burrows-Wheeler Aligner.[1] We employed the Picard software to remove PCR duplicates and evaluate the quality of variants. The Genome Analysis Toolkit was employed to call and analyze single-nucleotide variants (SNVs) and indels.[2] The SNVs with read depths less than 4× were filtered out. Then, functional information on genetic variants from the Gene Ontology Consortium, Sorting Intolerant From Tolerant (SIFT), Polymorphism Phenotyping v2 (PolyPhen-2), MutationTaster, the Exome Aggregation Consortium (ExAC) Browser and KEGG pathway databases were annotated through the ANNOVAR tool.[3-9] The Online Mendelian Inheritance in Man (OMIM) database was also used for functional annotation in this study.

Male infertility is potentially exposed to strong purifying selection because of the defects to natural conception. Therefore, the pathogenic variants responsible for MMAF cannot be common in the general populations. In this study, the genetic variants with allele frequencies ≥ 0.01 in the human population genome databases (e.g., the ExAC Browser and 1000 Genomes Project) were excluded.[9,10] Nonsense, frameshift and essential splice-site variants were preferred. Missense variants predicted to be deleterious by SIFT, PolyPhen-2, and/or MutationTaster were also included for further analyses. Previous studies have so far only demonstrated the autosomal recessive inheritance for human MMAF.[11] Therefore, homozygous or compound heterozygous variants were kept for further verification.

Semen Analysis

Semen samples of human subjects were collected by masturbation after 2-7 days of sexual abstinence, and were examined after liquefaction for 30 min at 37 ℃. Analyses of semen volume, sperm concentration, and motility were carried out and replicated in the source hospitals during routine biological examination according to the 5th World Health Organization (WHO) guidelines.

Sperm samples of mice were from the cauda epididymides, and were obtained by dissection of adult male mice followed by incubation in 1 mL solution of capacitation for 15 min at 37 ℃. Semen characteristics were evaluated using the computer-assisted sperm analysis (CASA) system.

Transmission Electron Microscopy

Semen samples were washed and fixed routinely, and then were progressively dehydrated with graded ethanol (50%, 70%, 90%, and 100%) and 100% acetone. After drying and embedding, the specimens were sliced with ultra-microtome and stained with uranyl acetate and lead citrate. The slices were observed and photographed by TEM (TECNAI-10, Philips) with an accelerating voltage of 80 kV.

Supplemental References

1. Li, H., and Durbin, R. (2010). Fast and accurate long-read alignment with Burrows-Wheeler transform. Bioinformatics *26*, 589-595.
2. McKenna, A., Hanna, M., Banks, E., Sivachenko, A., Cibulskis, K., Kernytsky, A., Garimella, K., Altshuler, D., Gabriel, S., Daly, M., et al. (2010). The Genome Analysis Toolkit: a MapReduce framework for analyzing next-generation DNA sequencing data. Genome Res. *20*, 1297-1303.
3. Wang, K., Li, M., and Hakonarson, H. (2010). ANNOVAR: functional annotation of genetic variants from high-throughput sequencing data. Nucleic Acids Res. *38*, e164.
4. Ashburner, M., Ball, C.A., Blake, J.A., Botstein, D., Butler, H., Cherry, J.M., Davis, A.P., Dolinski, K., Dwight, S.S., Eppig, J.T., et al. (2000). Gene ontology: tool for the unification of biology. The Gene Ontology Consortium. Nat. Genet. *25*, 25-29.
5. Kanehisa, M., Furumichi, M., Tanabe, M., Sato, Y., and Morishima, K. (2017). KEGG: new perspectives on genomes, pathways, diseases and drugs. Nucleic Acids Res. *45*, D353-D361.
6. Kumar, P., Henikoff, S., and Ng, P.C. (2009). Predicting the effects of coding non-synonymous variants on protein function using the SIFT algorithm. Nat. Protoc. *4*, 1073-1081.
7. Adzhubei, I.A., Schmidt, S., Peshkin, L., Ramensky, V.E., Gerasimova, A., Bork, P., Kondrashov, A.S., and Sunyaev, S.R. (2010). A method and server for predicting damaging missense mutations. Nat. Methods *7*, 248-249.
8. Schwarz, J.M., Cooper, D.N., Schuelke, M., and Seelow, D. (2014). MutationTaster2: mutation prediction for the deep-sequencing age. Nat. Methods *11*, 361-362.
9. Lek, M., Karczewski, K.J., Minikel, E.V., Samocha, K.E., Banks, E., Fennell, T., O'Donnell-Luria, A.H., Ware, J.S., Hill, A.J., Cummings, B.B., et al. (2016). Analysis of protein-coding genetic variation in 60,706 humans. Nature *536*, 285-291.
10. 1000 Genomes Project Consortium, Abecasis, G.R., Auton, A., Brooks, L.D.,

DePristo, M.A., Durbin, R.M., Handsaker, R.E., Kang, H.M., Marth, G.T., and McVean, G.A. (2012). An integrated map of genetic variation from 1,092 human genomes. Nature *491*, 56-65.

11. Ben Khelifa, M., Coutton, C., Zouari, R., Karaouzene, T., Rendu, J., Bidart, M., Yassine, S., Pierre, V., Delaroche, J., Hennebicq, S., et al. (2014). Mutations in DNAH1, which encodes an inner arm heavy chain dynein, lead to male infertility from multiple morphological abnormalities of the sperm flagella. Am. J. Hum. Genet. *94*, 95-104.